Journal of Materials Chemistry B

PAPER

View Article Online
View Journal

Cite this: DOI: 10.1039/c4tb01501k

Siderophore-inspired nanoparticle-based biosensor for the selective detection of Fe^{3+}†

Daniel J. Phillips,[a] Gemma-Louise Davies[a] and Matthew I. Gibson*[ab]

Received 10th September 2014
Accepted 5th November 2014

DOI: 10.1039/c4tb01501k

www.rsc.org/MaterialsB

Inspired by nature's exploitation of the 1,2-dihydroxybenzene unit (or catechol) in mammalian and bacterial siderophores, we report the first example of a nanoparticle sensing system that utilises the strong catechol–Fe^{3+} binding motif to trigger nanoparticle aggregation, promoting a powerful optical response. Gold nanoparticles are functionalised with RAFT polymerisation-prepared water-soluble poly(*N*-hydroxyethyl acrylamide) containing a catechol moiety at the α-chain-end. A strong red-to-purple colorimetric response occurs in the presence of Fe^{3+} at serum concentrations (8–25 μM) in saline solution. Sodium chloride is critical in generating a strong optical output, as is the length of polymer used to coat the AuNPs. This behaviour is also demonstrated to be selective for Fe^{3+} over a host of other biologically relevant ions.

Introduction

Iron is the most abundant metal in the body with the average adult requiring around 5 g, using it for a range of functions including oxygen transport, electron transport and a variety of metabolic processes.[1] The *in vivo* concentration is however carefully regulated to avoid serious health implications. For example, a common anaemia is caused by insufficient dietary intake and absorption of iron, whilst elevated iron concentrations, such as those present in genetic disorders such as hemochromatosis, can produce excess levels of Reactive Oxygen Species *via* Fenton chemistry.[2,3] Undesirable iron levels have also been linked to a variety of diseases including Alzheimer's and Parkinson's,[4] making the effective detection of iron species a critical area of study.

The ability to sequester iron in the human body is complicated by the poor bioavailability of the ferric ion (Fe^{3+}), which predominates in aerobic conditions, exhibiting compounds with poor aqueous solubility of approximately 10^{-18} M.[5] To overcome this, it is sequestered within the porphyrin ring of heme and as a co-factor in haemoglobin and myoglobin, whilst its passage into cells depends heavily on transport proteins such as transferrin.[6,7] Bacteria also require sufficient levels of the metal to survive and grow, abstracting it from their mammalian hosts with siderophores – low molecular weight complexes that bind iron with an association constant in excess of 10^{50} – allowing effective competition with the host for iron sequestration.[7,8]

A large number of bacterial siderophores are known in comparison to the single mammalian siderophore, siderocalin,[6] which sequesters the bacterial siderophore–iron complex to prevent bacterial uptake.[9–11] The majority of these species are divided into three groups: α-hydroxycarboxylates, hydroxamates and catecholates. These functionalities have inspired the development of a number of compounds such as deferoxamine, deferiprone and deferasirox for use in iron chelation therapies,[12,13] and have provided a focus for investigations into the use of siderophore-mimics as pharmaceutical and antibiotic drug targeting devices.[14,15]

The development of sensors capable of detecting a variety of metal ions is a popular field of research.[16,17] A variety of detection platforms/responses can be used, including proteins and DNA,[18,19] field-effect transistor devices,[20–22] photonic crystals,[23] metal electrodes,[24,25] plasmonic resonance energy transfer-based nanospectroscopy[26] and graphene oxide,[27] whilst the ability to trigger a fluorescent response upon metal ion binding has received significant study.[28,29] A particularly attractive platform is that of gold nanoparticles (AuNPs) due to their facile preparation, control over size, ease of surface functionalisation through simple coating strategies and, most importantly for sensing applications, their varying optical properties.[30–32] Specifically, the extent of nanoparticle dispersion/aggregation has a significant effect on the nanoparticle colour due to shifts in surface plasmon resonance (SPR). This signature has been applied for the detection of a variety of metal ions including lithium,[33] mercury,[34,35] potassium,[36] aluminium,[37] lead[38] and chromium.[39] However, there are few instances of the application of AuNPs capable of detecting iron that have been reported.

[a]Department of Chemistry, University of Warwick, Gibbet Hill Road, Coventry, CV4 7AL, UK. E-mail: m.i.gibson@warwick.ac.uk; Fax: +44 (0)2476524112; Tel: +44 (0) 2476524803

[b]Warwick Medical School, University of Warwick, Gibbet Hill Raod, Coventry, CV4 7AL, UK

† Electronic supplementary information (ESI) available: Experimental details, additional small molecule, polymer and gold nanoparticle characterisation; additional data as described in main text. See DOI: 10.1039/c4tb01501k

Bai *et al.* functionalised gold nanoparticles with a hydrophilic ligand, to ensure water solubility, and a 4-piperazinyl-1,8-naphthalimide-based ligand which was able to complex with Fe^{3+}, generating a colorimetric and fluorescent output.[40] Mehta *et al.* have used *p*-amino salicylic acid dithiocarbamate functionalised gold nanoparticles as colorimetric probes for the detection of Fe^{3+} in both aqueous and urine samples.[41] Tripathy *et al.* have prepared a colorimetric detection system based on gold, where the addition of Fe^{3+} in the presence of thiourea and hydrochloric acid catalyses leaching of the gold, damping the SPR and hence resulting in a visible colour change.[42] Wu *et al.* have functionalised gold nanoparticles with pyrophosphate which underwent a pink-to-violet change in the presence of Fe^{3+}, showing excellent selectivity for Fe^{3+} over a host of other ions.[43]

Inspired by the structure and action of siderophores, we hypothesised that the binding between catechols, the key functional group in siderophores synthesised mainly by bacteria,[44] and Fe^{3+} may be sufficient to affect the aggregation behaviour of a gold nanoparticle suspension in order to generate an optical response. To date, catechol groups have been used in the formulation of nanoparticles as a way of stabilising the metallic cores, but not as a means of preparing nanoparticles whereby the catechol unit is available to undergo further chemistry. For instance, their use in stabilising iron oxide nanoparticles is obvious given the affinity between the two.[45] Catechol groups have been grafted onto mesoporous silica nanoparticles[46] and have also been used as a stabiliser in the synthesis of gold nanoparticles from their parent Au(III) salt due to the redox chemistry involved in the interchange of catechol to quinone species.[47–49] To the best of our knowledge however, there are few examples whereby (gold) nanoparticles have been prepared with a catechol group protruding from the particle surface, allowing active use.[50]

Developments in controlled radical polymerisation (CRP) methodologies over the past two decades have enabled the routine generation of vast arrays of polymeric architectures with high levels of control over functionality, chain-end structure and topology. Moreover, polymers derived from the Reversible Addition-Fragmentation Chain Transfer (RAFT) methodology[51] are ideally suited for further reaction with gold nanoparticles given the inherent affinity between gold and the thiol groups derived from the ω-end of the preceding polymer chains.[32] Herein, inspired by the structure and biological importance of siderophores, we detail the first example of a gold nanoparticle system capable of sensing physiologically relevant Fe^{3+} concentration through the powerful catechol–Fe^{3+} binding motif.

Results and discussion

Catechol-functional polymers

To prepare catechol-functional polymers, a new chain-transfer agent (CTA) was synthesised based on an adaptation of the method described by Zobrist *et al.*[52] First, the carboxylic acid-terminated trithiocarbonate **1** was activated using standard coupling chemistry (*N*-hydroxysuccinimide (NHS)/*N*,*N*′-diisopropylcarbodiimide (DIC)) to give compound **2**. This was then reacted with a slight excess of dopamine hydrochloride (Dop·HCl), in the presence of triethylamine (TEA), to furnish **3** in good yield (Scheme 1). Importantly, the product could be isolated by precipitation in hexane, negating the need for column chromatography which may be complicated by the presence of an unprotected catechol unit. Moreover, no by-product generated by aminolysis of the trithiocarbonate[53,54] was observed, as confirmed ^{1}H, ^{13}C NMR, FTIR and HRMS (Fig. S1–S3, ESI†).

Catechol-functional Au nanoparticles

To effectively furnish catechol-functional gold nanoparticles, a water-soluble polymer was first required. Hence, *N*-hydroxyethyl acrylamide (HEA) was polymerised using CTA **3** and 4,4′-azobis(4-cyanovaleric acid), ACVA, as thermal initiator. This polymer was also deliberately chosen as it does not possess thermo-responsive behaviour and hence removes any potential complication of particle aggregation behaviour given the transition temperature of thermo-responsive polymers is known to change when tethered to gold nanoparticles.[55] The polymerisation conditions used afforded rapid polymerisation rates (at least 75% conversion after 35 minutes) and polymers with a range of molecular weights were prepared and characterised by SEC and ^{1}H NMR (Table 1, Fig. S4, ESI†). Narrow dispersities (≤1.20) were observed, an attractive feature of the RAFT technique.

Nanoparticles can be routinely synthesised from Au^{3+} salts and are ideally suited for RAFT-derived polymers given the strong affinity between thiols, which are derived from the ω-trithiocarbonate terminus, and gold. This can be used to prepare self-assembled monolayers and has been previously exploited to generate large nanoparticle libraries.[56] Commercially-available citrate-stabilised nanoparticles with a diameter of 40 nm (**AuNP$_{40}$**) were used as a starting material and coated with the polymers by a simple mixing procedure, washing several times by centrifugation to remove excess polymer, to yield **pHEA-1/2/3@AuNP$_{40}$** (Scheme 1).

Successful functionalisation of the nanoparticles was confirmed by several techniques. UV-visible spectrophotometry revealed a distinctive blue shift in maximum wavelength from 525 nm for the uncoated particles to between 531–534 nm following polymer addition, implicit of a change in the

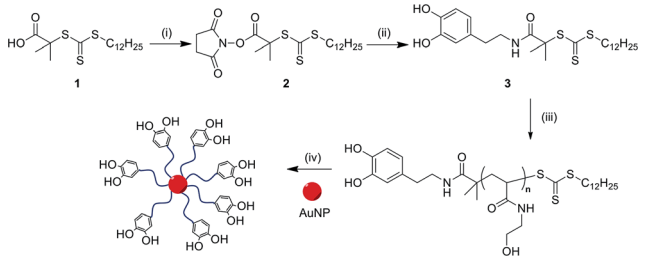

Scheme 1 Synthetic scheme for preparation of catechol-functional gold nanoparticles (**pHEA-1/2/3@AuNP$_{40}$**): (i) NHS/DIC, THF, 0 °C → r.t, 16 h; (ii) Dop·HCl/TEA, MeOH, r.t, 48 h; (iii) HEA, 3, ACVA, MeOH/toluene, 70 °C, 35 min; (iv) polymer/AuNP, 5 °C, 16 h.

Table 1 Poly(*N*-hydroxyethyl acrylamide) samples prepared

Polymer	[M] : [CTA]	Conversion[a] (%)	M_n[a] (th) (g mol^{-1})	M_n[b] (SEC) (g mol^{-1})	M_w/M_n[b]
pHEA-1	30	83.1	2900	4800	1.14
pHEA-2	75	78.5	6800	9700	1.17
pHEA-3	200	74.7	17200	17500	1.20
pHEA-4	75	74.1	6400	10200	1.16

[a] Determined by ^{1}H NMR relative to an internal standard (mesitylene). [b] Determined by SEC (DMF inc. 5 mM NH_4BF_4) relative to PMMA standards.

refractive index of the coating (Fig. S5A, ESI†). DLS analysis also indicated an increase in particle size from 41.5 ± 0.2 nm for the uncoated particles to between 80 and 126 nm when polymer-coated, with the size increasing as polymer length increases (Table 2, Fig. S5, ESI†). TEM confirmed core particle sizes of ~40 nm (Table 2, Fig. S6, ESI†) with narrow size distributions in all cases. Due to the low degrees of surface loading and low EM contrast relative to gold, the surface polymer coating was not clearly observed by this technique (Fig. S6, ESI†). Particle sizes by DLS are larger for polymer-coated particles due to the presence of the hydrophilic polymer layer contributing to the particles' hydrodynamic diameter as the functionalised particles undergo Brownian motion, as well as hydrogen bonding and van der Waals interactions between neighbouring particles. The larger particle sizes observed for **pHEA-1/2@AuNP$_{40}$** by DLS may suggest a small degree of aggregation resulting during the polymer coating process. However, given the lack of a significant colour change to either purple/blue (associated with large-scale AuNP aggregation) or colourless (associated with AuNP precipitation), these particles were still deemed sufficiently dispersed for further testing.

Selective Fe^{3+} detection

These catechol-functionalised nanoparticles were then probed for their ability to detect Fe^{3+} in aqueous solution. Two points of reference are often used to assess changes in the aggregation behaviour of gold: (i) any change in maximum SPR_{max}, where aggregation results in a shift to longer wavelengths and (ii) any change in absorbance at 700 nm (Abs@700 nm), which may also be accompanied by a decrease in intensity of SPR_{max}.[57] **PHEA-2@AuNP$_{40}$** was incubated with varying concentrations (100 μM–1 nM) of $FeCl_3 \cdot 6H_2O$ for 30 min in a 50 mM NaCl solution at room temperature and the UV/visible spectrum between 450 and 700 nm was measured (Fig. 1A). Notably, in the presence of 10 μM Fe^{3+}, a shift in SPR_{max} from 532 nm to 547 nm was observed, together with an increase in Abs@700 nm from 0.288 to 0.602. Interestingly, minimal response was seen in the presence of any other iron concentration (*vide infra*). It was found that the absence of salt in the nanoparticle suspension resulted in a lack of detectable change in their optical properties (Fig. 1B). This was not entirely unexpected, since the modulation of ionic strength has been known to tune particle aggregation *via* interparticle electrostatic repulsion.[58,59]

This ionic-concentration behaviour was further tuned by fixing the concentration of $FeCl_3 \cdot 6H_2O$ at 10 μM and varying the concentration of NaCl in the AuNP suspensions up to saline concentration (150 mM). Fig. 2A demonstrates a noticeable, non-linear increase in both SPR_{max} and Abs@700 nm with increasing levels of NaCl. This is likely due to an increased screening of any negative charge on the particle surface caused by residual citrate or the catecholate complex, allowing greater interparticle interactions. The initial Fe^{3+} assay (Fig. 1) was thus repeated in 150 mM NaCl (saline) and similar optical shifts were observed, but with amplified behaviour (SPR_{max} shifted by 20 nm and Abs@700 nm by 0.412 compared to the absence of salt) due to the ionic environment (Fig. 2B). As the optical responses in 150 mM NaCl were significantly larger, providing a noticeable change in appearance (Fig. 2A inset), these conditions were employed in the rest of the study. Particle stability over time in 150 mM NaCl was confirmed by DLS (Fig. S7, ESI†).

Interestingly, a linear trend in SPR_{max} and Abs@700 nm with increasing Fe^{3+} concentration is not observed. There is a

Table 2 Characterisation of gold nanoparticles used

Code	DLS diameter (nm)	TEM diameter (nm)	SPR_{max} (nm)
AuNP$_{40}$ (uncoated)	41.5 ± 0.2	36.2 ± 3.8	525
pHEA-1@AuNP$_{40}$	126.0 ± 2.6	38.0 ± 4.4	534
pHEA-2@AuNP$_{40}$	113.7 ± 3.2	39.0 ± 4.1	532
pHEA-3@AuNP$_{40}$	79.5 ± 0.4	38.2 ± 2.8	531
pHEA-4@AuNP$_{40}$	59.6 ± 3.5	37.5 ± 4.0	530

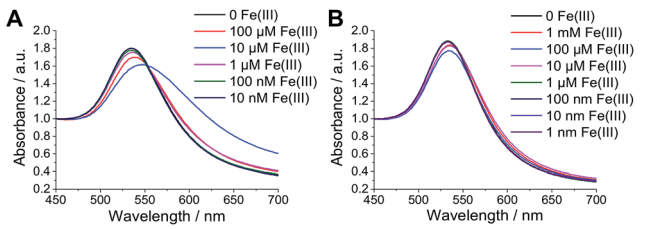

Fig. 1 Response of **pHEA-2@AuNP$_{40}$** in the presence of various concentrations of Fe^{3+} and (A) 50 mM NaCl, (B) 0 M NaCl.

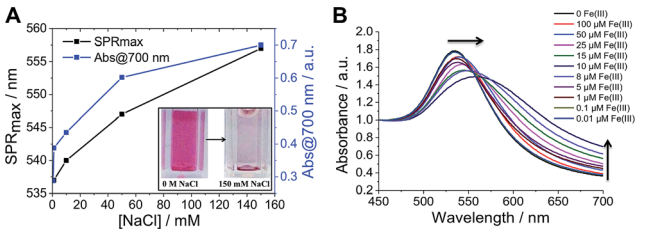

Fig. 2 (A) Change in SPR_{max} and Abs@700 nm of **pHEA-2@AuNP$_{40}$** in the presence of 10 μM Fe^{3+} as a function of NaCl concentration. Inset shows the appearance of **pHEA-2@AuNP$_{40}$** in the presence of 10 μM Fe^{3+} and either 0 or 150 mM NaCl. (B) UV/visible spectra demonstrating response of **pHEA-2@AuNP$_{40}$** in 150 mM NaCl to various concentrations of Fe^{3+}.

noticeable increase with increasing Fe^{3+} concentration up to a concentration of 10 μM; however, further increases in concentration led to a decreased optical response (Fig. 3A). The fact that the same general trend is observed for both SPR_{max} and Abs@700 indicates the applicability of both measurements as a tool for assessing the aggregation behaviour of AuNPs.

Aggregation behaviour was confirmed by DLS analysis (Fig. 3B). A significant increase in particle size was first observed at 10 μM Fe^{3+}, peaking at 25 μM Fe^{3+}, before decreasing when the concentration reached 100 μM. This trend at Fe^{3+} concentrations greater than 100 μM is likely due to increased Coulombic repulsions as a result of excess Fe^{3+} ions.[40] The change in particle size and the change in Abs@700 nm with respect to iron concentration yielded very similar trends (Fig. 3B). This is indicative of aggregation due to catechol–Fe^{3+} binding rather than due to non-specific response of the polymer chains.

Several control studies were carried out to further confirm that the observed response was due to selective catechol–Fe^{3+} binding. Incubation of **pHEA-2@AuNP$_{40}$** in 150 mM NaCl with $FeCl_2 \cdot 4H_2O$ resulted in no significant change in either SPR_{max} or Abs@700 nm. A slight increase in Abs@700 nm was observed with increasing Fe^{2+} (difference of 0.076 with 100 μM Fe^{2+}) which may be due to reduced stability of these particles leading to the beginnings of a "salting-out" type phenomenon (Fig. S8, ESI†). The binding of catecholate-based siderophores to Fe^{2+} is significantly weaker than that of Fe^{3+} due to the reduced charge density on the coordinated cation.[8] This is important as one of the main known mechanisms for the release of iron from siderophores comprises the reduction of siderophore-bound Fe^{3+} to Fe^{2+} followed by spontaneous release or competitive sequestration of this reduced species.[60]

A polymer of similar molecular weight containing a phenyl end-group was prepared as a negative control to directly compare with the catechol end-group containing polymers (**pHEA-4**, Table 1, Fig. S8, ESI†). AuNPs were functionalised with **pHEA-4** using the same coating technique (**pHEA-4@AuNP$_{40}$**, Table 2) to yield particles with a diameter of 59.6 ± 3.5 nm (DLS). Incubation with Fe^{3+} revealed no response to any concentration tested, proving that the catechol end-group is necessary to promote cross-linking and hence optical responsive behaviour (Fig. S8, ESI†). A summary of the incubation of **pHEA-2/4@AuNP$_{40}$** with Fe^{2+} and Fe^{3+} is shown in Scheme 2.

In a bid to further tune the selectivity of the nanoparticles to the presence of iron, the effect of polymer molecular weight on aggregation behaviour was investigated. AuNPs coated with a short polymer (molecular weight ~3000 g mol^{-1}; **pHEA-1@AuNP$_{40}$**) showed poor saline stability, with aggregation and precipitation occurring within 30 minutes, even at low NaCl concentrations, and a colour change from red/pink to blue/purple (Fig. 4A). This precipitation is most likely due to the shorter polymer chain failing to offer sufficient steric stabilisation in the presence of the electrolyte.

Coating the particles with a longer polymer (molecular weight ~17 000 g mol^{-1}; **pHEA-3@AuNP$_{40}$**) provided good saline stability, however no aggregation occurred at any Fe^{3+} concentration (Fig. 4B). The importance of polymer linker length on AuNP-based detection systems has been demonstrated previously: Richards *et al.* demonstrated that glycosylated AuNPs, designed for the detection of FimH positive bacteria, required the addition of a poly(ethylene glycol) spacer between the nanoparticle core and carbohydrate extremity in order to increase saline stability and specificity for bacterial binding.[57]

Finally, the Fe^{3+} specificity of the nanocomposites was investigated by carrying out a comparative assay with a range of biologically relevant cations (Fig. 5). The optical response of our

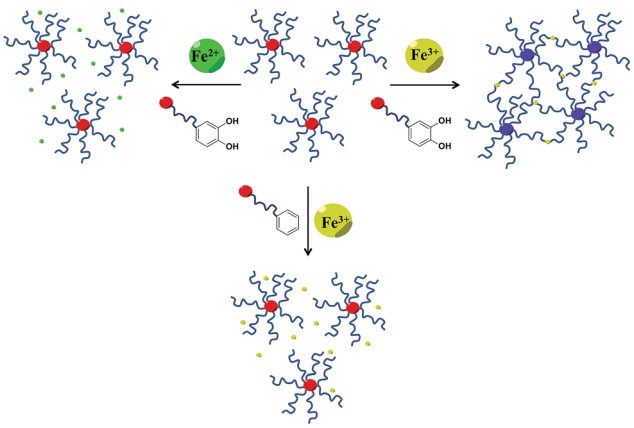

Scheme 2 Gold nanoparticles functionalised with catechol or phenyl end-groups and their response to Fe^{2+} and Fe^{3+}. Dispersed and aggregated particles have red and purple colours respectively, representative of the optical absorbance changes observed experimentally.

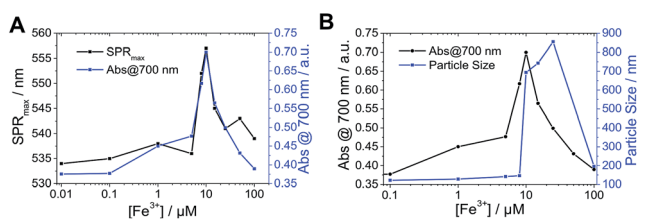

Fig. 3 Response of **pHEA-2@AuNP$_{40}$** in 150 mM NaCl to various concentrations of Fe^{3+}: (A) SPR_{max} and Abs@700 nm and (B) comparison of Abs@700 nm (UV/vis) and particle size (DLS) as a function of Fe^{3+} concentration.

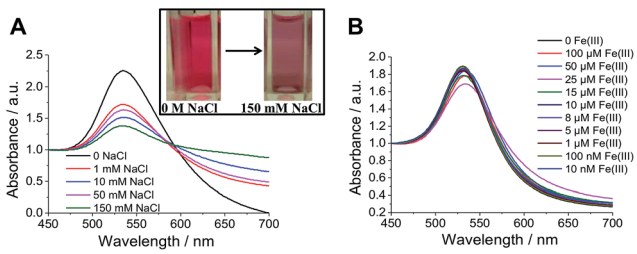

Fig. 4 (A) UV/visible spectra showing response of **pHEA-1@AuNP$_{40}$** to NaCl (inset: appearance at 0 and 150 mM NaCl); (B) UV/visible spectra showing response of **pHEA-3@AuNP$_{40}$** to various concentrations of Fe^{3+}.

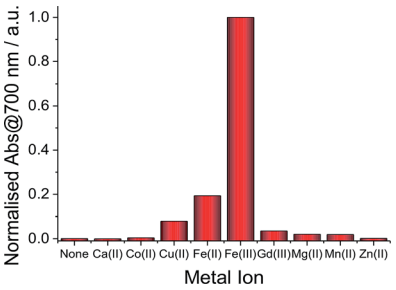

Fig. 5 Response of **pHEA-2@AuNP$_{40}$**, doped with 150 mM NaCl, to a variety of metal cations.

optimised nanoparticulate system, as assessed by the change in Abs@700 nm, was over 10-fold stronger in the presence of Fe^{3+} than the majority of ions tested. Some binding and optical changes were observed in the presence of Fe^{2+}, which is likely due to the partial oxidation to Fe^{3+} over the duration of the assay test. A minimal response was observed in the presence of Gd^{3+}, another tribasic metal ion, further highlighting the specificity of a catechol unit to Fe^{3+}.

Conclusions

Inspired by nature's need for iron acquisition, this study presents the first example using the strong catechol–Fe^{3+} binding motif as a route to manipulating the dispersion/aggregation behaviour of gold nanoparticles as optical sensing devices. A small library of water-soluble poly(*N*-hydroxyethyl acrylamide) was prepared using an α-chain end, catechol-functional chain transfer agent. These polymers were subsequently used to coat commercially-available 40 nm gold nanoparticles and characterised by a range of techniques. The propensity for catechol–Fe^{3+} binding was then assessed using simple UV/visible spectrophotometry and DLS-based assays. The addition of salt was observed to be critical in the observation of particle aggregation, due to successful shielding of residual negative charge on the AuNP surface. The response was dependent on the amount of salt used in a non-linear fashion, with physiologically-relevant saline conditions (150 mM NaCl) providing the best response in terms of both optical SPR_{max} band shifting and the observed Abs@700 nm.

With these optimised conditions, a selective response of the gold nanoparticle system to Fe^{3+} concentrations between 8 and 25 μM was achieved, with the most notable visual response occurring with 10 μM Fe^{3+}. Concentrations above and below this gave minimal indication of aggregation by DLS and UV/visible spectrophotometry. It is suggested that in this current system, a trade-off exists between adding sufficient concentration of Fe^{3+} to trigger nanoparticle cross-linking and an excess which promotes Coulombic repulsion. Nevertheless, this limitation is minimal given the iron concentrations detected in this current system correspond to those found in human serum.[61] The length of polymer chain on the extent of iron response was also optimised; small chains failed to provide sufficient steric stability resulting in rapid aggregation in even very low concentrations of NaCl, whilst long chains failed to generate any noticeable response due to increased steric stability. Finally, the nature and specificity of the aggregation behavior was shown, notably giving between a 5- and 10-fold higher response to Fe^{3+} than other biologically relevant cations tested.

Our system exhibits an optimal optical response between 8–25 μM Fe^{3+}, offering valuable sensing potential as serum iron concentration is also in this range.[61] Ongoing work is focused on tailoring the nanoparticle surface/surrounding environment to promote a response to a wider range of Fe^{3+} concentrations for use as a sensor in both deprived and iron-rich conditions. Furthermore, the sensitivity of the catechol moiety to solution pH, where differing degrees of complexation (mono, bis and tris-catecholate species) are known[62] is being pursued with a view to even greater system tuning. Finally, the application of this nano-bio sensory system in more complex biological media is also ongoing.

Acknowledgements

Equipment used was supported by the Innovative Uses for Advanced Materials in the Modern World (AM2), with support from Advantage West Midlands (AWM) and part funded by the European Regional Development Fund (ERDF). MIG is a Birmingham Science City Interdisciplinary Research Fellow funded by the Higher Education Funding Council for England (HEFCE). DJP thanks the University of Warwick for a scholarship. GLD acknowledges the Institute for Advanced Study (Warwick) for a Global Research Fellowship, the Royal Society, the Medical and Life Sciences Research Fund (Warwick) and the General Charities of the City of Coventry for Bursaries supporting this research.

Notes and references

1 E. L. Que, D. W. Domaille and C. J. Chang, *Chem. Rev.*, 2008, **108**, 1517–1549.
2 N. C. Andrews, *N. Engl. J. Med.*, 1999, **341**, 1986–1995.
3 C. C. Winterbourn, *Toxicol. Lett.*, 1995, **82–83**, 969–974.
4 A. I. Bush, *Curr. Opin. Chem. Biol.*, 2000, **4**, 184–191.
5 T. Zheng and E. M. Nolan, *Metallomics*, 2012, **4**, 866–880.
6 C. Correnti and R. K. Strong, *J. Biol. Chem.*, 2012, **287**, 13524–13531.
7 E. P. Skaar, *PLoS Pathog.*, 2010, **6**, e1000949.
8 R. C. Hider and X. Kong, *Nat. Prod. Rep.*, 2010, **27**, 637–657.
9 D. H. Goetz, M. A. Holmes, N. Borregaard, M. E. Bluhm, K. N. Raymond and R. K. Strong, *Mol. Cell*, 2002, **10**, 1033–1043.
10 T. H. Flo, K. D. Smith, S. Sato, D. J. Rodriguez, M. A. Holmes, R. K. Strong, S. Akira and A. Aderem, *Nature*, 2004, **432**, 917–921.
11 B. E. Allred, C. Correnti, M. C. Clifton, R. K. Strong and K. N. Raymond, *ACS Chem. Biol.*, 2013, **8**, 1882–1887.
12 P. V. Bernhardt, *Dalton Trans.*, 2007, 3214–3220.
13 N. Hanspeter, *Curr. Opin. Chem. Biol.*, 2007, **11**, 419–423.
14 Y. Lu and M. J. Miller, *Bioorg. Med. Chem.*, 1999, **7**, 3025–3038.

15 U. Möllmann, L. Heinisch, A. Bauernfeind, T. Köhler and D. Ankel-Fuchs, *BioMetals*, 2009, **22**, 615–624.
16 Z. Liu, W. He and Z. Guo, *Chem. Soc. Rev.*, 2013, **42**, 1568–1600.
17 R. D. Hancock, *Chem. Soc. Rev.*, 2013, **42**, 1500–1524.
18 Y. Xiang and Y. Lu, *Inorg. Chem.*, 2013, **53**, 1925–1942.
19 S. Wen, T. Zeng, L. Liu, K. Zhao, Y. Zhao, X. Liu and H.-C. Wu, *J. Am. Chem. Soc.*, 2011, **133**, 18312–18317.
20 E. S. Forzani, X. Li, P. Zhang, N. Tao, R. Zhang, I. Amlani, R. Tsui and L. A. Nagahara, *Small*, 2006, **2**, 1283–1291.
21 O. Knopfmacher, M. L. Hammock, A. L. Appleton, G. Schwartz, J. Mei, T. Lei, J. Pei and Z. Bao, *Nat. Commun.*, 2014, **5**, DOI: 10.1038/ncomms3954.
22 T. Nguyen Duc, R. El Zein, J.-M. Raimundo, H. Dallaporta and A. M. Charrier, *J. Mater. Chem. B*, 2013, **1**, 443–446.
23 B.-F. Ye, Y.-J. Zhao, Y. Cheng, T.-T. Li, Z.-Y. Xie, X.-W. Zhao and Z.-Z. Gu, *Nanoscale*, 2012, **4**, 5998–6003.
24 X. Luo, A. Morrin, A. J. Killard and M. R. Smyth, *Electroanalysis*, 2006, **18**, 319–326.
25 J. Gooding, D. Hibbert and W. Yang, *Sensors*, 2001, **1**, 75–90.
26 Y. Choi, Y. Park, T. Kang and L. P. Lee, *Nat. Nanotechnol.*, 2009, **4**, 742–746.
27 Q. Mei, C. Jiang, G. Guan, K. Zhang, B. Liu, R. Liu and Z. Zhang, *Chem. Commun.*, 2012, **48**, 7468–7470.
28 K. P. Carter, A. M. Young and A. E. Palmer, *Chem. Rev.*, 2014, **114**, 4564–4601.
29 D. W. Domaille, E. L. Que and C. J. Chang, *Nat. Chem. Biol.*, 2008, **4**, 168–175.
30 G. Doria, J. Conde, B. Veigas, L. Giestas, C. Almeida, M. Assunção, J. Rosa and P. V. Baptista, *Sensors*, 2012, **12**, 1657–1687.
31 M. Grzelczak, J. Perez-Juste, P. Mulvaney and L. M. Liz-Marzan, *Chem. Soc. Rev.*, 2008, **37**, 1783–1791.
32 J. Shan and H. Tenhu, *Chem. Commun.*, 2007, 4580–4598.
33 S. O. Obare, R. E. Hollowell and C. J. Murphy, *Langmuir*, 2002, **18**, 10407–10410.
34 C.-J. Yu and W.-L. Tseng, *Langmuir*, 2008, **24**, 12717–12722.
35 Z. Jiang, Y. Fan, M. Chen, A. Liang, X. Liao, G. Wen, X. Shen, X. He, H. Pan and H. Jiang, *Anal. Chem.*, 2009, **81**, 5439–5445.
36 G. Patel, A. Kumar, U. Pal and S. Menon, *Chem. Commun.*, 2009, 1849–1851.
37 S. Chen, Y.-M. Fang, Q. Xiao, J. Li, S.-B. Li, H.-J. Chen, J.-J. Sun and H.-H. Yang, *Analyst*, 2012, **137**, 2021–2023.
38 J. Liu and Y. Lu, *J. Am. Chem. Soc.*, 2003, **125**, 6642–6643.
39 Y.-C. Chen, I. L. Lee, Y.-M. Sung and S.-P. Wu, *Sens. Actuators, B*, 2013, **188**, 354–359.
40 L. Bai, L. Zhu, C. Y. Ang, X. Li, S. Wu, Y. Zeng, H. Ågren and Y. Zhao, *Eur. J. Chem.*, 2014, **20**, 4032–4037.
41 V. N. Mehta, S. K. Kailasa and H.-F. Wu, *New J. Chem.*, 2014, **38**, 1503–1511.
42 S. K. Tripathy, J. Y. Woo and C.-S. Han, *Sens. Actuators, B*, 2013, **181**, 114–118.
43 S.-P. Wu, Y.-P. Chen and Y.-M. Sung, *Analyst*, 2011, **136**, 1887–1891.
44 W. S. Kaim, B. Schwederski and A. Klein, *Inorganic Biochemistry: Inorganic Elements in the Chemistry of Life*, John Wiley & Sons, Ltd., Chichester, 2013.
45 A. K. L. Yuen, G. A. Hutton, A. F. Masters and T. Maschmeyer, *Dalton Trans.*, 2012, **41**, 2545–2559.
46 Y. Zhu, H. S. Sundaram, S. Liu, L. Zhang, X. Xu, Q. Yu, J. Xu and S. Jiang, *Biomacromolecules*, 2014, **15**, 1845–1851.
47 K. C. L. Black, Z. Liu and P. B. Messersmith, *Chem. Mater.*, 2011, **23**, 1130–1135.
48 G. Marcelo and M. Fernandez-Garcia, *RSC Adv.*, 2014, **4**, 11740–11749.
49 Y. Lee, S. H. Lee, J. S. Kim, A. Maruyama, X. Chen and T. G. Park, *J. Controlled Release*, 2011, **155**, 3–10.
50 T. Inomata, T. Murase, H. Ido, T. Ozawa and H. Masuda, *Chem. Lett.*, 2014, **43**, 1146–1148.
51 J. Chiefari, Y. K. Chong, F. Ercole, J. Krstina, J. Jeffery, T. P. T. Le, R. T. A. Mayadunne, G. F. Meijs, C. L. Moad, G. Moad, E. Rizzardo and S. H. Thang, *Macromolecules*, 1998, **31**, 5559–5562.
52 C. d. Zobrist, J. Sobocinski, J. l. Lyskawa, D. Fournier, V. r. Miri, M. Traisnel, M. Jimenez and P. Woisel, *Macromolecules*, 2011, **44**, 5883–5892.
53 D. J. Phillips and M. I. Gibson, *Biomacromolecules*, 2012, **13**, 3200–3208.
54 H. Willcock and R. K. O'Reilly, *Polym. Chem.*, 2010, **1**, 149–157.
55 M. I. Gibson, D. Paripovic and H.-A. Klok, *Adv. Mater.*, 2010, **22**, 4721–4725.
56 M. I. Gibson, M. Danial and H.-A. Klok, *ACS Comb. Sci.*, 2011, **13**, 286–297.
57 S.-J. Richards, E. Fullam, G. S. Besra and M. I. Gibson, *J. Mater. Chem. B*, 2014, **2**, 1490–1498.
58 H. Zhang and D. Wang, *Angew. Chem., Int. Ed.*, 2008, **47**, 3984–3987.
59 S.-i. Yusa, K. Fukuda, T. Yamamoto, Y. Iwasaki, A. Watanabe, K. Akiyoshi and Y. Morishima, *Langmuir*, 2007, **23**, 12842–12848.
60 M. Miethke and M. A. Marahiel, *Microbiol. Mol. Biol. Rev.*, 2007, **71**, 413–451.
61 R. S. Porter, *The Merck Manual Home Health Handbook*, Merck Research Laboratories, Whitehouse Station, NJ, USA, 2009.
62 N. Holten-Andersen, M. J. Harrington, H. Birkedal, B. P. Lee, P. B. Messersmith, K. Y. C. Lee and J. H. Waite, *Proc. Natl. Acad. Sci. U. S. A.*, 2011, **108**, 2651–2655.

